Eur. J. Mineral., 35, 645–658, 2023
https://doi.org/10.5194/ejm-35-645-2023

European Journal of Mineralogy
Open Access

Provenance, protolith and metamorphic ages of jadeite-bearing orthogneiss and host paragneiss at Tavagnasco, the Sesia Zone, Lower Aosta Valley, Italy

Jane A. Gilotti[1], William C. McClelland[1], Simon Schorn[2], Roberto Compagnoni[3], and Matthew A. Coble[4,5]

[1]Department of Earth and Environmental Sciences, University of Iowa, Iowa City, IA 52242, USA
[2]NAWI Graz Geocenter, University of Graz, 8010 Graz, Austria
[3]Department of Earth Sciences, University of Torino, 10125 Turin, Italy
[4]Department of Geological Sciences, Stanford-USGS Ion Microprobe Laboratory, Stanford, CA 94305, USA
[5]Department of Environmental Chemistry, GNS Science, Avalon, 5010, New Zealand

Correspondence: Jane A. Gilotti (jane-gilotti@uiowa.edu)

Received: 25 April 2023 – Revised: 30 June 2023 – Accepted: 5 July 2023 – Published: 15 August 2023

Abstract. An eclogite-facies orthogneiss and host paragneiss from a quarry near Tavagnasco in the Lower Aosta Valley were studied in order to refine the protolith, provenance and metamorphic ages of the Eclogitic Micaschist Complex of the Sesia Zone. The orthogneiss contains jadeite with quartz + phengite + K-feldspar ± garnet + rutile + zircon, whereas the paragneiss hosts garnet + jadeite + phengite ± glaucophane + epidote + rutile + quartz. Phase diagram modeling of two representative samples yields minimum equilibration conditions of 550 ± 50 °C and 18 ± 2 kbar. Cathodoluminescence images of zircon from the orthogneiss show oscillatory-zoned cores that are embayed and overgrown by complex, oscillatory-zoned rims. Four concordant secondary ion mass spectrometry analyses from the cores give a weighted mean ^{206}Pb / ^{238}U age of 457 ± 5 Ma. The cores have Th/U = 0.1 and negative Eu anomalies indicative of an igneous protolith, which we interpret to have crystallized in the Ordovician at 780 °C, based on Ti-in-zircon measurements. Zircon rims yield a range of ^{206}Pb / ^{238}U dates from 74 to 86 Ma, and four concordant analyses define a weighted mean ^{206}Pb / ^{238}U age of 78 ± 2 Ma. The rims are interpreted to have grown in the eclogite facies based on their lower Th/U (0.01), less negative Eu anomalies and steeper heavy rare earth element (HREE) patterns at < 600 °C. The paragneiss yielded a detrital zircon population with major peaks at 575–600, 655 and 765 Ma; minor older components; and a maximum depositional age of approximately 570 Ma. The prominent Neoproterozoic zircon population and Ediacaran depositional age suggest derivation from the Gondwana margin. The metamorphic zircon is consistent with the oldest eclogite-facies event in the Sesia Zone; it does not show evidence of multiple periods of rim growth or any pre-Alpine (e.g., Variscan) metamorphism.

1 Introduction

The arcuate Western Alps record the oblique collision and continental subduction of the European plate beneath the Adriatic plate from the Late Cretaceous onwards (Dal Piaz, 2001; Beltrando et al., 2010a; Handy et al., 2010). Recent profiles based on seismic tomography depict a fossil subduction channel (Malusà et al., 2021; Paul et al., 2022) left over from the Alpine collision in which fragments of the ultrahigh-pressure (UHP) metamorphic units of European plate affinity (e.g., Dora-Maira) and Piemonte–Liguria Ocean (e.g., Lago di Cignana) were formed and exhumed. Adria, the overriding plate in the Western Alps, exhibits an older – sometimes called early Alpine – high-pressure (HP) metamorphic history starting in the Cretaceous, with blueschists and eclogites common in the thrust sheets of the Dent Blanche–Sesia tectonic system (Angiboust et al., 2014; Manzotti et al., 2014a). The Sesia Zone and Dent Blanche

units are thought to be derived from the distal margin of Adria, where most authors view them as fragments of hyperextended continental crust (Beltrando et al., 2010b, 2014). High-pressure metamorphism occurred during eastward subduction of some of these rifted fragments (Manzotti et al., 2014a) and/or subduction erosion of the distal Adriatic margin (Polino et al., 1990; Angiboust et al., 2014).

The timing of early Alpine HP metamorphism in the continental units of Adria spans at least 25×10^6 years (Manzotti et al., 2014a), with eclogite formation occurring between 85–60 Ma in the Sesia Zone alone. Unraveling the age of the HP metamorphism is important to reconstructing the tectonic evolution of subduction in the Alps. Timing is complicated by having different slices metamorphosed at different times (e.g., Regis et al., 2014), as well as some slices metamorphosed in multiple subduction–exhumation cycles (e.g., Rubatto et al., 2011). Although mapping is incomplete, progress is being made to identify individual tectonic slices based on recognizing the shear zones that bound them (Angiboust et al., 2014; Giuntoli and Engi, 2016), as well as the different fabrics within them (Babist et al., 2006). The Sesia Zone provides a clear example that the long time span of HP metamorphism is punctuated by episodic events recording complex flow within a subduction channel that requires a concentrated geochronological effort to solve.

This study focuses on the earliest eclogite-facies event recorded in the Western Alps by continental crust of the Sesia Zone, specifically a jadeite-bearing orthogneiss hosted by jadeite-bearing paragneiss. Pressure–temperature (P–T) conditions for the peak P assemblage are estimated with the aid of isochemical phase equilibrium models. We utilize secondary ion mass spectrometry (SIMS) U–Pb dating of zircon to refine earlier estimates (Liermann et al., 2002) of the age of the protolith and subsequent HP metamorphism of a jadeite-bearing orthogneiss that were obtained with thermal ion mass spectrometry (TIMS) methods. We also present detrital zircon ages from the eclogite-facies schist that forms the host rock to the orthogneiss. The results elucidate the depositional and plutonic history of the protolith, as well as bolster the ages of eclogite-facies metamorphism from continental crust of Adria.

2 Geological setting

The Sesia Zone (Fig. 1) is a composite unit dominated by a late Paleozoic crystalline basement that is traditionally divided into three main map units based on lithology and metamorphic grade: the Eclogitic Micaschist Complex, the Gneiss Minuti Complex and the Second Diorite–Kinzigite Zone (Compagnoni et al., 1977). Other structural divisions that identify separate thrust slices are also in use (e.g., Manzotti et al., 2014b; Giuntoli and Engi, 2016). The Sesia Zone is bound to the east by the Canavese Zone and the Ivrea Zone, consisting of thin slices of mantle-derived and crustal rocks that escaped the Alpine overprint. Units belonging to the Piemonte–Liguria Ocean lie directly to the south and west. The Dent Blanche unit is a large klippe of Adrian continental crust that overlies the oceanic rocks and is part of a tectonic unit that includes the Sesia Zone (Manzotti et al., 2014a). Map units below and to the west of the Piemonte–Liguria Ocean (Fig. 1a) are affiliated with the European plate.

The rocks in this study are from the Eclogitic Micaschist Complex, which consists of a polydeformed and polymetamorphic basement comprised of mica schist and paragneiss, minor metamafic rock (now eclogite), orthogneiss, and impure marble. This basement was intruded by abundant Carboniferous to Permian granitoids, such as the Monte Mucrone granitoid (Compagnoni and Maffeo, 1973), and minor gabbros (Bussy et al., 1998; Rubatto, 1998). Older Silurian–Devonian intrusives of leucomonzogranitic composition have also been recognized (Liermann et al., 2002). A Mesozoic sedimentary cover – with paragneiss, carbonate schist and locally manganiferous impure quartzite – has been reported from the central part of the Eclogitic Micaschist Complex (Venturini et al., 1994). During the Alpine orogeny, the Eclogitic Micaschist Complex variably recrystallized under quartz eclogite-facies conditions at peak $P < 20$ kbar and $T < 600$ °C (Tropper et al., 1999; Zucali et al., 2002). A pervasive greenschist-facies retrogression overprints the eclogite-facies parageneses near the contact with the Gneiss Minuti Complex (Compagnoni et al., 1977, 2013), but much of the HP metamorphism in the Eclogitic Micaschist Complex is very well preserved.

The age of early Alpine HP metamorphism in the Eclogitic Micaschist Complex is bracketed between ca. 85–65 Ma (Regis et al., 2014) with different ages of peak P recognized in different parts of the Sesia Zone. Older ages (85–75 Ma) are prevalent in the east, while younger cycles of eclogite-facies metamorphism occur from 75–65 Ma in the west (Rubatto et al., 2011; Regis et al., 2014). These ages are bracketed by an older phase of HP metamorphism (110–85 Ma) in the Austroalpine nappes of Switzerland and Austria, also thought to be part of Adria, and the younger HP and UHP metamorphism of the Zermatt–Saas units belonging to the Piemonte–Liguria Ocean (Manzotti et al., 2014a, and references therein). The pattern shows a clear younging of HP metamorphism towards the European continent during the Alpine collision.

3 Sample description

We studied jadeite-bearing samples collected near Tavagnasco in the Lower Aosta Valley (Fig. 1b) in order to improve on the ages obtained by TIMS for the leucomonzogranitic magmatic protolith and the HP metamorphism of the orthogneiss (Liermann et al., 2002). The jadeite-bearing orthogneiss is exploited in two quarries and marketed with the trade name *Verde Argento*, which trans-

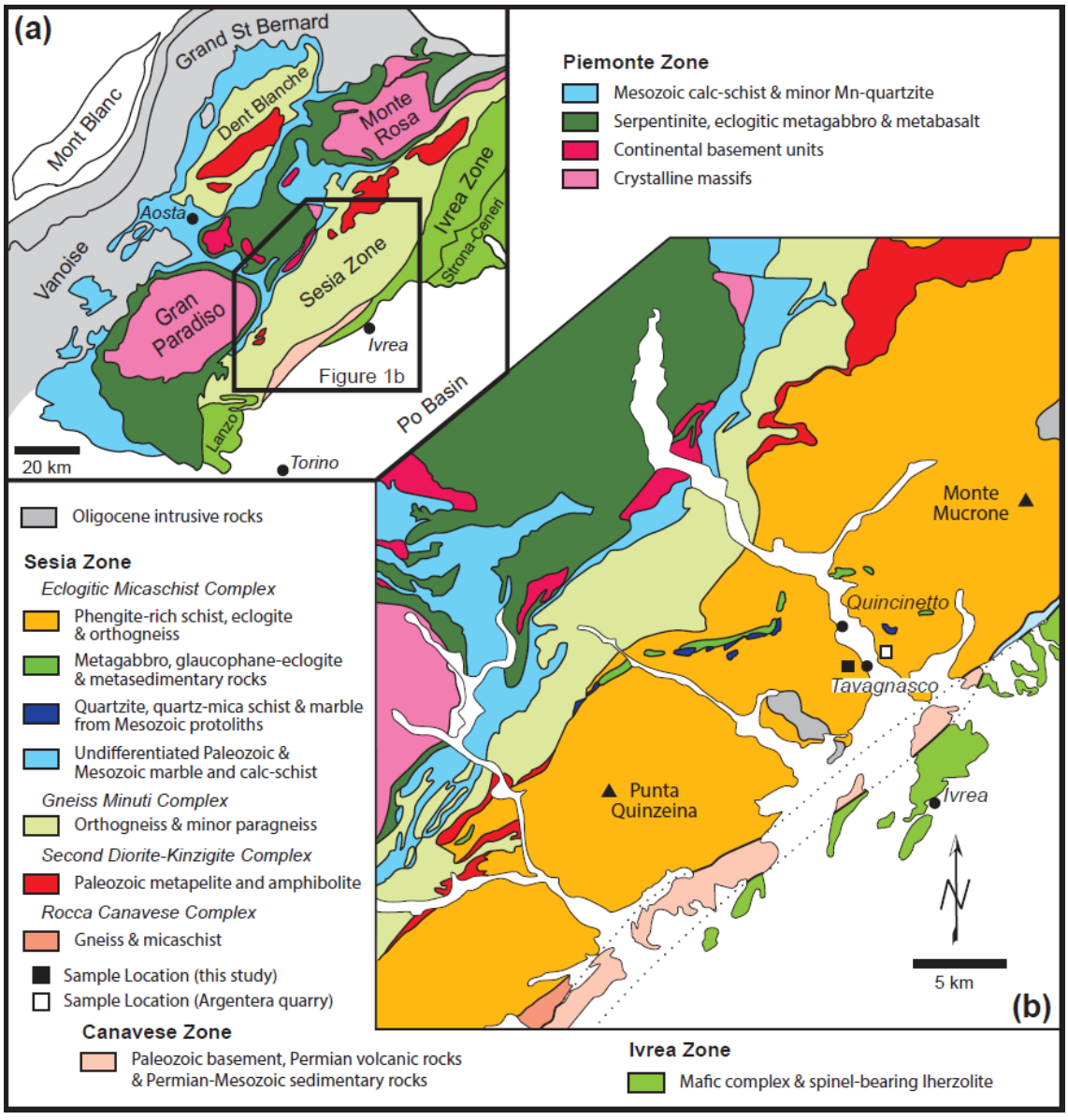

Figure 1. Simplified geological maps showing **(a)** the Western Alps and **(b)** the sample location near the village of Tavagnasco within the Sesia Zone. Maps adapted from Compagnoni et al. (2013).

lates to silvery green (Fiora et al., 1999). The orthogneiss forms a whitish layer up to a few tens of meters thick that is isoclinally folded with a horizontal axial plane (Compagnoni et al., 2013). The two quarries are separated across the Aosta Valley by 2.5 km, but they are part of the same coherent orthogneiss layer. A typical hand sample of the orthogneiss contains white K-feldspar and quartz, pale green jadeite, and flakes of dark green phengite (Fig. 2). In other places, especially near the orthogneiss selvages, the jadeite forms rounded porphyroclasts up to 5 cm in diameter, giving the gneiss an augen-like texture or conglomeratic appearance, with perhaps the best example exposed on Le Colme mountain (Andreoli et al., 1976). Orthogneiss sample 15-1 consists mainly of quartz, jadeite, K-feldspar and phengite (Fig. 3) with minor glaucophane and garnet; accessory Al-rich titanite; metamict allanite, zircon and apatite; and local fluorite, calcite and Fe sulfide. Jadeite is commonly rimmed by a retrograde corona of albite and thin flakes of paragonite (Fig. 3a, b). Tropper et al. (1999) used this rock to calibrate the jadeite–K-feldspar–quartz barometer, which is useful for determining P in eclogite-facies metagranitoids and metapelites.

Jadeite-bearing paragneiss hosts the leucomonzogranitic intrusions. The paragneiss is compositionally layered on the centimeter to decimeter scale, with layers recognized by the abundance or scarcity of white mica (Fig. 2c, d). Sam-

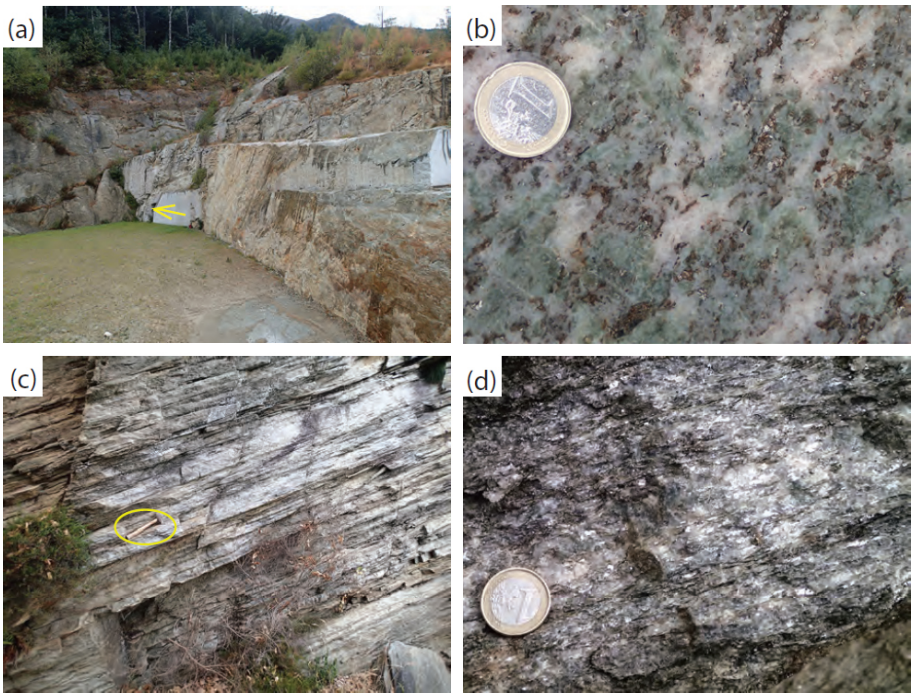

Figure 2. Outcrop photographs. **(a)** The quarry west of Tavagnasco; arrow marks the location of sample 15-1. **(b)** The *Verde Argento* leucocratic orthogneiss; the green mineral is jadeite. **(c)** The metasedimentary host rocks (paragneiss) beneath the orthogneiss in the quarry. Sample 15-2 was taken at the hammer. **(d)** Close-up of phengite–jadeite–quartz schist sample 15-2. Coin is 2.3 cm in diameter.

ple 15-2, collected for provenance analysis on the road below the quarry, is an extremely zircon-rich mica schist. The paragneiss consists of the eclogite-facies assemblage: quartz, phengite, small atoll-like garnet, poikiloblastic jadeite, epidote, accessory rutile and retrograde albite (Fig. 3c). A second paragneiss sample, VA1, was collected from the same quarry as 15-1 because it contained glaucophane in addition to jadeite (Fig. 3d) and hence was more amenable to thermodynamic modeling.

4 Analytical methods

Samples collected for zircon U/Pb geochronology were processed at the University of Iowa to obtain heavy mineral separates by standard crushing, density and magnetic separation techniques. U–Th–Pb isotopes and trace elements in zircon from the igneous sample were analyzed by SIMS using the sensitive high-resolution ion microprobe with reverse geometry (SHRIMP-RG) instrument at the Stanford-USGS Micro-Analysis Center, Stanford, California. U–Th–Pb data from detrital zircon in the metasedimentary sample were obtained by laser ablation inductively coupled plasma mass spectrometry (LA-ICP-MS) at the Arizona LaserChron Center, Tucson, Arizona.

Table 1. Bulk rock chemistry.

	XRF bulk (wt %)		Model bulk (mol %)	
Sample	VA-1	15-1	VA-1	15-1
SiO_2	68.43	74.98	74.99	83.30
TiO_2	0.84	0.07	0.69	0.06
Al_2O_3	13.35	13.39	8.62	8.76
Fe_2O_3	5.44	1.28	–	–
FeO^{tot}	–	–	4.49[c]	1.07[c]
MnO	0.09	0.03	0.08	–
MgO	2.22	0.09	3.63	0.16
CaO	1.93[a]	0.46[a]	2.02[b]	0.07[b]
Na_2O	2.94	3.38	3.12	3.63
K_2O	2.26	4.09	1.58	2.90
P_2O_5	0.16	0.31	–	–
LOI	1.21	0.88	–	–
O	–	–	0.79[d]	0.05[d]
Total	98.87	98.96	100.00	100.00
$X_{Fe^{3+}}$	–	–	0.35[e]	0.10[e]

[a] Whole-rock CaO^{tot}.
[b] Corrected for P_2O_5 in apatite ($= CaO^{tot} - 3.33 \times P_2O_5$).
[c] FeO^{tot} is total Fe expressed as FeO.
[d] 0.5 $FeO_{1.5}$.
[e] $X_{Fe^{3+}} = 2 \times O/FeO^{tot} = Fe^{3+}/(Fe^{3+} + Fe^{2+})$.

4.1 Bulk rock and mineral chemistry

Whole-rock bulk composition was determined by X-ray fluorescence (XRF) using a Bruker Pioneer S4 XRF instrument housed at the NAWI Graz Geocenter, University of Graz (Table 1). Fusion discs were prepared from whole-rock powders following standard procedures. Analyses were calibrated using approximately 60 international reference samples; reference material GSP-2 was routinely analyzed as a precision monitor.

Backscattered electron (BSE) images and mineral compositions were acquired using a JEOL JXA-8530Fplus HyperProbe electron probe microanalyzer (EPMA), equipped with one energy dispersive and five wavelength dispersive spectrometers, located at the NAWI Graz Geocenter, University of Graz. Analyses were obtained with a 15 kV acceleration voltage, 10 nA probe current and a 1–5 µm spot size. Counting times were 5 s for background and 10 s for all elemental peaks. A range of synthetic and natural mineral standards were used for element calibration. Mineral formulae were calculated with the software PET 7 (Dachs, 1988). Key mineral chemistry data are reported in Table S1 in the Supplement. Mineral abbreviations follow Whitney and Evans (2010).

4.2 SIMS U–Pb geochronology

Zircon from sample 15-1 was mounted in epoxy with geochronology reference materials R33 (420 Ma; Black et al., 2004; Mattinson, 2010) and MAD-559 (3940 µg g^{-1} U; Coble et al., 2018) for U/Pb fractionation and concentration corrections. The mount was polished to expose the grain interiors and imaged by cathodoluminescence (CL) using an in-house detector mounted on a JEOL 5600 scanning electron microscope (SEM) at Stanford University to guide spot placement in uniform domains. U–Th–Pb and rare earth element (REE) analysis using a spot size of 20 µm and trace element analysis using a 15 µm spot followed routines outlined in Barth and Wooden (2006, 2010). The systematic error including uncertainty in $^{206}Pb/^{238}U$ calibration based on repeated measurements of R33 was 1.7 % (2σ standard deviation). The $^{206}Pb/^{238}U$ ages were corrected for common Pb using the ^{207}Pb method (see Williams, 1998). Initial common Pb isotopic composition was approximated from Stacey and Kramers (1975). Data reduction and ages were calculated using the programs of Ludwig (2008, 2009). Trace element concentrations were calibrated against the zircon reference material MAD-559 (Coble et al., 2018). The estimated errors (1σ) for trace elements based on repeated analysis of MAD-559 are 3 %–10 %. Titanium had an estimated error of 4 % based on analysis of MAD-559. U/Pb data were plotted on Tera-Wasserburg diagrams using Isoplot 3.6 (Ludwig, 2008). Analytical results are presented in Table S2.

4.3 LA-ICP-MS detrital zircon analysis

Zircon for analysis at the Arizona LaserChron Center was mounted in epoxy with natural zircon reference materials SL (558 Ma, 518 µg g^{-1} U and 68 µg g^{-1} Th; Gehrels et al., 2008), R33 (420 Ma; Black et al., 2004; Mattinson, 2010) and FC (1099 Ma; Paces and Miller, 1993) and polished to expose the grain interiors. All samples were imaged with CL at the University of Iowa using a Gatan ChromaCL system mounted on a Hitachi 3500N SEM to see zonation and relict cores in individual grains and guide spot location. Mounts were cleaned prior to analysis with a 2 % HNO_3–1 % HCl solution. Grains were analyzed for U–Th–Pb isotopes using a Photon Machines Analyte G2 excimer laser with a HelEx ablation cell coupled with a Thermo Scientific Element 2 single collector HR-ICP-MS following analytical procedures outlined in Gehrels et al. (2008) and Gehrels and Pecha (2014). Analysis of reference materials SL, R33 and FC was used to determine U/Pb fractionation and concentration corrections. Analytical conditions and results of unknowns and reference materials with analytical or random uncertainties including the contributions from the measurement of $^{206}Pb/^{238}U$, $^{206}Pb/^{207}Pb$ and $^{206}Pb/^{204}Pb$ are reported in Table S3. The common Pb composition was estimated from Stacey and Kramers (1975). The systematic uncertainties, including contributions from analysis and age of reference materials and decay constants for ^{238}U and ^{235}U, are reported for the sample and added in quadrature to each analysis. Data reduction and plotting were done using programs at the Arizona LaserChron Center and Isoplot (Ludwig, 2008).

Detrital zircon analyses with > 10 % uncertainty (2σ analytical error) in the $^{206}Pb/^{238}U$ date, > 10 % uncertainty in the $^{207}Pb/^{206}Pb$ date for > 700 Ma and > 25 % uncertainty in the $^{207}Pb/^{206}Pb$ date for < 700 Ma are not included in the assessment of provenance or maximum depositional age (MDA). Analyses with > 10 % discordance or > 5 % reverse discordance are not included, with discordance based on the ratio $^{206}Pb/^{238}U$ date and $^{206}Pb/^{207}Pb$ date and analytical error propagated at the 2σ level following equations in Gibson et al. (2021). Obtained dates are interpreted as ages of individual grains in a detrital population. The "best age" is determined from the $^{206}Pb/^{238}U$ date for analyses with a $^{206}Pb/^{238}U$ date < 1200 Ma and from the $^{206}Pb/^{207}Pb$ date for analyses with a $^{206}Pb/^{238}U$ date > 1200 Ma. The MDA is estimated from the median value of the youngest age population calculated using the TuffZirc method (Ludwig, 2008), which also provides an evaluation of potential Pb loss based on the number of youngest grains excluded from the youngest population (Gehrels et al., 2020).

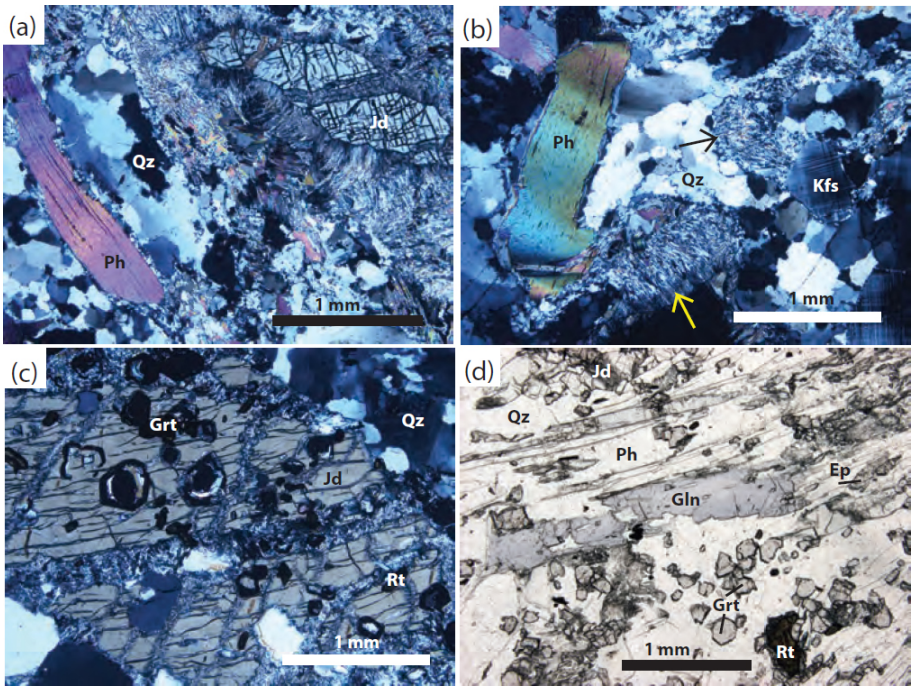

Figure 3. Photomicrographs of the jadeite-bearing orthogneiss and paragneiss. **(a)** Prismatic jadeite (Jd) with two cleavages at 90° partially replaced by a corona of albite + paragonite, cross polarized light (XPL), sample 15-1. **(b)** A more retrogressed part of the same thin section with large deformed phengite in dynamically recrystallized quartz. Jadeite is completely replaced by fine-grained albite + paragonite pseudomorphs (at arrows), XPL. **(c)** Jadeite porphyroblast contains atoll garnet in paragneiss 15-2. Fractures are filled with retrograde albite and paragonite, XPL. **(d)** Jadeite + glaucophane paragneiss VA1 in plane polarized light. Mineral abbreviations follow Whitney and Evans (2010).

5 Pressure–temperature estimates

5.1 Phase equilibrium modeling

Isochemical P–T phase diagrams (i.e., pseudosections) were computed using THERMOCALC v3.47 (Powell and Holland, 1988) and an updated version of the Holland and Powell (2011) dataset (file tc-ds62.txt, created 6 February 2012). The activity–composition models used are clinoamphibole and clinopyroxene (Green et al., 2016), muscovite–paragonite (White et al., 2014a), garnet (White et al., 2014b), plagioclase–K-feldspar (Holland and Powell, 2003), and epidote (Holland and Powell, 2011). We employed the omphacite model of Green et al. (2016), which allows for order–disorder on sites designed to simulate coexisting sub-solvus clinopyroxenes (i.e., diopside, omphacite, jadeite). The aluminosilicates, rutile, albite, quartz and H_2O are assumed to be pure phases. Phase abundances were calculated as mole fractions, with each phase normalized to one oxide sum total to approximate volume percent.

For the jadeite-glaucophane paragneiss (sample VA1), the whole-rock analysis was converted to the 11-component MnO–Na_2O–CaO–K_2O–FeO–MgO–Al_2O_3–SiO_2–H_2O–TiO_2–O_2 (MnNCKFMASHTO) model system. The model system for jadeite orthogneiss 15-1 omitted MnO, as this component is negligible in the garnet-absent rock. Of the total Fe, approx. 35 % is assumed to be Fe^{3+} for the paragneiss and 10 % for the orthogneiss. The Fe^{3+} values were chosen to roughly reproduce the measured X_{Fe} of the main silicates of the inferred equilibrium assemblage. Water saturation was assumed. Total CaO was reduced based on the amount of P_2O_5 that would sequester Ca in apatite. The model composition used in the calculations is given in Table 1. Pseudosections, calculated between 500–600 °C and 15–22 kbar, are presented in Fig. 4.

The inferred equilibrium assemblage of paragneiss VA1 is garnet + glaucophane + jadeite + muscovite (phengite) + epidote + rutile + quartz + H_2O, which is constrained by the disappearance of epidote towards high T and its replacement by lawsonite at high P, covering a large P–T range (Fig. 4a). At the lowest P–T considered, two sub-solvus clinopyroxenes coexist. The modeling predicts the stability of minor paragonite (∼ 4–8 vol %), which is inconsistent with petrological observations. The absence of paragonite in metapelites has been attributed to H_2O undersaturation (Massonne and Sobiech, 2007), which appears unlikely in this sample because of the abundance of hydrous minerals. The lack of paragonite may instead be due to imperfections in the predicted element partitioning between amphibole and clinopyroxene (Forshaw et al.,

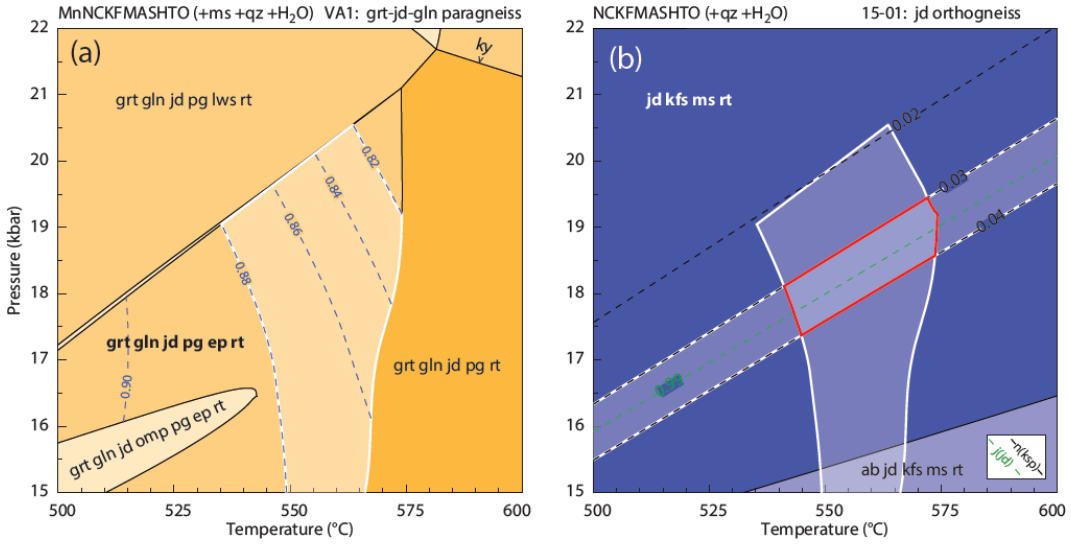

Figure 4. Pseudosections. **(a)** Estimate for P_{max} recorded by garnet–glaucophane–jadeite paragneiss VA1 and **(b)** jadeite orthogneiss 15-1. The inferred equilibrium assemblage is highlighted in bold white lines and shading. Dashed blue lines in **(a)** are contours for X_{Fe} in garnet. The kyanite-in curve is shown. The red box in **(b)** is the overlap of the most plausible P–T conditions recorded by both samples.

2019). Similarly, the measured mineral compositions (Table S1) are only poorly reproduced by the calculations. We therefore base our estimate of the potential equilibration conditions on the calculated stability field of the thin section assemblage. The respective demise and appearance of epidote and lawsonite, refined using isopleths for the X_{Fe} [$= Fe^{2+} / (Fe^{2+} + Mg)$] of garnet rims and small grains (0.82–0.88), yield conservative equilibration conditions of $T = 530$–$580\,°C$ and $P \leq 20\,kbar$ for paragneiss VA1.

Orthogneiss 15-1 contains the inferred equilibrium assemblage jadeite + muscovite (phengite) + K-feldspar + rutile + quartz + H_2O, existing over a large P–T range and limited variability in mineral composition (Fig. 4b). The lower P limit of the stability field is marked by the introduction of albite, and no strong constraints on T are available. Using the calculated j(cpx) [$= Na / (Na + Ca)$] of ~ 0.99 as indicative of P, the possible equilibration conditions of the orthogneiss are estimated using n (ksp) [$= Na / (Na + Ca + K)$] of K-feldspar $= 0.03$–0.04. Overlapping the refined stability fields of the two samples yields P–T conditions of $550 \pm 50\,°C$ and $18 \pm 2\,kbar$, assuming standard uncertainties.

5.2 Ti-in-zircon temperature

Ti-in-zircon temperatures were calculated using Ferry and Watson (2007), assuming the activity of SiO_2 is equal to 1 ($aSiO_2 = 1$) and activity of TiO_2 is approximately 0.7 ($aTiO_2 = 0.7$) for rutile-absent siliceous melts (Hayden and Watson, 2007). Uncertainties inherent in the Ti-in-zircon T estimates are roughly $\pm 50\,°C$ (Watson et al., 2006). As described below, zircon from orthogneiss 15-1 shows clear core and rim domains in CL images. The core domains give Ti-in-zircon T estimates of approximately 780 °C. Estimates for the rims are approximately 590 °C, consistent with the thermodynamic models for the metamorphic assemblage.

6 SIMS geochronology of zircon in the orthogneiss

Zircon from orthogneiss 15-1 displays lower U (188–1700 µg g^{-1}), CL-bright, oscillatory-zoned cores that are embayed and overgrown by higher U (1700–7462 µg g^{-1}), CL-dark rims with oscillatory and convolute zoning (Fig. 5). The multi-faceted grain morphology and textural evidence for embayment and dissolution at the boundary between core and rim domains were interpreted to reflect fluid-assisted zircon overgrowth at high-pressure, low-temperature conditions (Liermann et al., 2002). U/Pb trace element analysis targeted specific CL domains to establish protolith versus metamorphic age populations. Of the seven core analyses (Table S2), five overlapping concordant analyses from the cores give a weighted mean $^{206}Pb / ^{238}U$ age of 457 ± 5 Ma (2σ; MSWD $= 0.1$), and two core analyses gave younger dates interpreted to record core–rim mixtures or domains with Pb loss (Fig. 5). The cores have Th/U $= 0.1$ and negative Eu anomalies (Eu/Eu* $= 0.01$) typical of igneous zircon. An Ordovician crystallization age is inferred for the protolith. The rim analyses define a range of ^{207}Pb-corrected $^{206}Pb / ^{238}U$ ages from 74 to 86 Ma. Four concordant analyses define a weighted mean $^{206}Pb / ^{238}U$ age of 78 ± 2 Ma (2σ; MSWD $= 2.7$). The rims have lower Th/U (0.01), less negative Eu anomalies (Eu/Eu* $= 0.1$–0.2) and steeper heavy REE (HREE) patterns (Yb/Gd $= 112$–157) that largely reflect depletion of light REEs (LREEs) with the exception of Ce. These trends are consistent with metamor-

phic zircon rim growth in the absence of garnet and presence of plagioclase in the assemblage at $T = 590\,^{\circ}\mathrm{C}$.

7 Detrital zircon geochronology of the paragneiss

Paragneiss 15-2 yielded abundant elongate to equant zircon with rim–core relationships similar to zircon from the adjacent orthogneiss. Cores are euhedral to rounded, typically oscillatory zoned and overgrown by 1 to 30 µm thick rims that have coarse oscillatory and convolute zoning in CL images (Fig. 6). Variation in CL textures in many of the grains records multiple periods of rim growth. The rims impart a multi-faceted subrounded external morphology to the grains. Spot placement guided by CL imaging targeted 105 cores for provenance evaluation and 5 rims or grains with CL zoning typical of the rims to determine the age of metamorphic overgrowths. A total of 48 out of 105 core analyses pass acceptance criteria based on discordance and uncertainties of both the $^{206}\mathrm{Pb}/^{238}\mathrm{U}$ and $^{207}\mathrm{Pb}/^{206}\mathrm{Pb}$ dates. Three analyses that are younger than orthogneiss 15-1 are interpreted to record Pb loss or mixed ages due to metamorphism. The remaining ages range from 520 to 2610 Ma and define major peaks at 570–600, 655 and 765 Ma with minor peaks at 875, 985 and 2005 Ma. The youngest group of analyses defines a TuffZirc $^{206}\mathrm{Pb}/^{238}\mathrm{U}$ age of 584 ± 19 Ma ($n = 10$) which is interpreted as the maximum depositional age for the sedimentary protolith (Fig. 6b). Discordant analyses are consistent with this pattern but suggest older components as well (Fig. 6d). Strongly discordant analyses define linear arrays with $^{207}\mathrm{Pb}/^{206}\mathrm{Pb}$ ages as old as 3.3 Ga. The observed discordance is interpreted to reflect the combined effects of Pb loss in the original detrital grains and analysis of mixed metamorphic and detrital domains. The four youngest rim analyses are mutually overlapping and concordant with $^{206}\mathrm{Pb}/^{238}\mathrm{U}$ dates ranging from 78 to 83 Ma (Fig. 6c). The large ($> 25\,\%$) 2σ uncertainty in calculated $^{207}\mathrm{Pb}/^{206}\mathrm{Pb}$ dates is typical of young (< 100 Ma) grains analyzed by LA-ICP-MS. Accepting this limitation, the rim analyses define a weighted mean $^{206}\mathrm{Pb}/^{238}\mathrm{U}$ age of 81 ± 4 Ma (Fig. 6c) that is consistent with the SHRIMP age of 78 ± 2 Ma for HP metamorphic rims on zircon in the adjacent orthogneiss.

8 Discussion and conclusions

8.1 Sedimentary provenance

Neoproterozoic sedimentary protoliths of the Sesia Zone, representing the western Southern Alpine domain of Adria, are inferred to lie within a belt of peri-Gondwanan terranes stretching along the northern Gondwana margin (Nance et al., 2008; Linnemann et al., 2008; von Raumer et al., 2015; Arboit et al., 2019). The minimum depositional age of 585 Ma for paragneiss 15-2 overlaps with representative ages of the Pan-African and Cadomian orogens (e.g., Linnemann et al., 2008). The broad array of peaks is consistent with derivation from Gondwanan basement sources including the West African Craton, Trans-Saharan belt, Saharan Metacraton and Arabian–Nubian shield (Avigad et al., 2015; Meinhold et al., 2021; Žák et al., 2022). Although the zircon signatures are significantly disturbed by metamorphism, the new results from the Sesia Zone are similar to provenance ages from other portions of Adria (e.g., Sirevaag et al., 2016; Siegesmund et al., 2023) and confirm the assumed ties between the Sesia Zone and the Neoproterozoic Gondwana margin. Future study of detrital zircon age and chemical characteristics for paragneiss units in the Eclogitic Micaschist Complex may help us to refine the paleogeographic affinities of, and tectonic boundaries between, various tectono-metamorphic slices proposed for the Sesia Zone.

8.2 Ordovician magmatism

The age of most igneous protoliths in the Western Alps has long been assumed to be Carboniferous–Permian on the basis of the widespread occurrence of granitoids and metagranitoids associated with Variscan orogenesis (e.g., Finger et al., 1997). However, Ordovician–Silurian (480–450 Ma) ages have been recognized in many parts of the pre-Mesozoic basement of the Alpine realm (Schaltegger and Gebauer, 1999; von Raumer et al., 2013, and references therein). Ordovician magmatism documented in the Sesia Zone is limited. Rb/Sr whole-rock ages of ~ 450 Ma from the Monte Emilius klippe provided the first evidence (Hunziker, 1974). The jadeite-bearing orthogneiss found in the quarries near Tavagnasco (Fig. 1b) subsequently gave upper intercept U/Pb TIMS ages of 435 ± 8 and 396 ± 21 Ma from samples HPG1 and HPG2, respectively, of Liermann et al. (2002). The new SIMS age of 457 ± 5 Ma from this study refines the earlier estimate from HPG1. Chen et al. (2023) re-examined the jadeite-bearing orthogneiss at the Argentera quarry, where HPG2 was collected, and produced a range of concordant SIMS dates from 436 ± 6 to 480 ± 7 Ma on zircon cores. They assign a protolith age of 459 ± 5 Ma to the sample based on coupled LA-ICP-MS U–Pb and trace element analysis. The intrusive age of the leucomonzogranitic protolith to the orthogneiss dated here (15-1) and by Chen et al. (2023) is consistent with the timing of Early Ordovician arc magmatism on the northern Gondwana margin (von Raumer et al., 2013; Zurbriggen, 2015). The results confirm the presence of coeval felsic magmatism from the Sesia Zone to the external basement massifs in the Western Alps. In addition, the results highlight the ongoing difficulty in resolving protolith ages from crystalline rocks subjected to continental subduction.

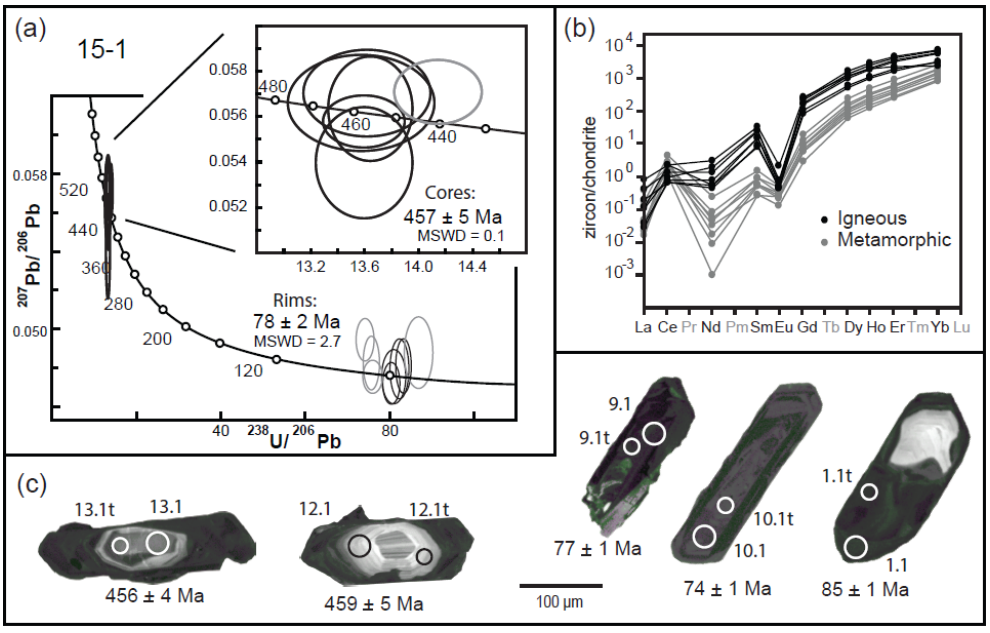

Figure 5. SIMS results from zircon in orthogneiss: **(a)** Tera-Wasserburg plot for analyzed zircon from sample 15-1 with an inset for the igneous cores. **(b)** Trace elements for zircon cores and rims. **(c)** Representative CL images of zircon showing clear distinction between core and rim domains, as well as analytical spot locations; *t* signifies trace element spot.

8.3 Variscan metamorphism

Paleozoic and older units preserved in the Alps are generally expected to have experienced medium- to high-grade metamorphism related to the Variscan orogeny (e.g., von Raumer et al., 2013). Basement units in the Western Alps also experienced widespread high-temperature metamorphism in the Permian (Kunz et al., 2018). The samples examined in this study do not record the Carboniferous–Permian metamorphism. Igneous and detrital protolith grains appear to be directly overgrown by Alpine eclogite-facies rims. The lack of preserved Paleozoic metamorphic zircon in the Sesia Zone has been documented by several studies (Rubatto et al., 2011; Regis et al., 2014) despite the numerous examples of Carboniferous–Permian zircon rims in samples of eclogitic mica schist. Detrital zircon from metasedimentary samples across the Eclogitic Micaschist Complex show the growth of single or multiple Permian rims with ages of 290–280 Ma that are in some cases overgrown by Cretaceous outer rims (Kunz et al., 2018; Vho et al., 2020). Regis et al. (2014) observed limited zircon rim growth at 354 ± 18 Ma prior to more voluminous Alpine rim growth. The absence of older rims does not establish a lack of Variscan metamorphism in the protolith because the preservation of older zircon rims is demonstrably local.

8.4 Conditions and timing of early Alpine HP metamorphism

Rubatto et al. (2011) provide clear evidence of two cycles of HP metamorphism and exhumation recorded by a single mica schist sample based on multiple generations of allanite, zircon, white mica and garnet. These authors obtained the oldest age for HP metamorphism in the Eclogitic Micaschist Complex – a SIMS $^{206}Pb / ^{238}U$ age of 78.5 ± 0.9 Ma – from zircon containing inclusions of HP minerals in zones defined by CL images and trace element patterns, which is the preferred method to tie dates to the *P–T* path (McClelland and Lapen, 2013). Regis et al. (2014) subsequently obtained a $^{232}Th / ^{208}Pb$ age on allanite of ca. 85 Ma from HP chloritoid-kyanite-garnet mica schists that corroborates an older phase of HP metamorphism in the Sesia Zone. The age of the zircon rims from orthogneiss 15-1 compares well with the 78.5 Ma HP rims from Rubatto et al. (2011). Both samples show steep HREE patterns but differ in the persistence of a slight negative Eu anomaly in the orthogneiss. Rims from another mica schist give an age of 76.8 ± 0.9 Ma and have flat HREE patterns consistent with HP growth (Rubatto et al., 2011). New data from an orthogneiss sample collected in the Argentera quarry suggest that zircon rims grew at 76.0 ± 1.0 Ma under UHP conditions (Chen et al., 2023). These authors link newly discovered coesite preserved in garnet with a flattened HREE pattern in zircon that shows a decrease in Yb and Lu. Steeper HREE patterns in zircon from their orthogneiss sample are similar to those observed in sample 15-1 but give an age of 74.1 ± 1.9 Ma (Chen et

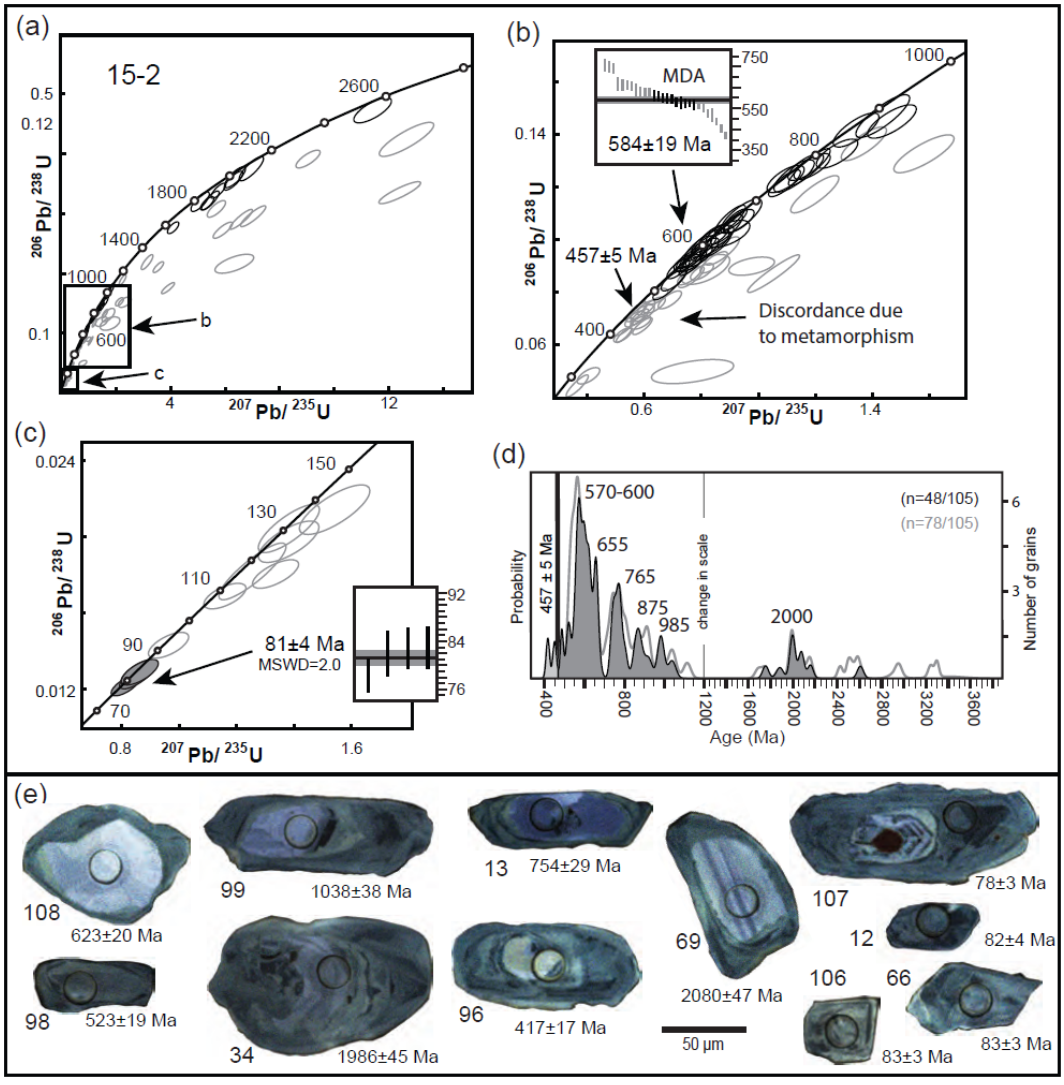

Figure 6. Sample 15-2. **(a)** Concordia diagram of detrital zircon showing analyses that pass (black ellipses) or fail (gray ellipses) the discordance and uncertainty filters and locations for plots in **(b)** and **(c)**. Errors shown at the 2σ level in all plots. **(b)** Concordia plot showing transition from $< 10\,\%$ (black) to $> 10\,\%$ (gray) discordant data in relation to the orthogneiss age of 457 ± 5 Ma. Inset shows analyses ($n = 10$) included in the calculation of the maximum depositional age using the TuffZirc method (Ludwig, 2008). **(c)** Concordia plot of young analyses that gives a metamorphic age of 81 ± 4 Ma. **(d)** Probability density plot of the detrital zircon population. The filled curve was calculated with n being the total number of analyses that were $< 10\,\%$ discordant and $< 5\,\%$ reversely discordant. Note the change in scale at 1200 Ma. **(e)** CL images of representative zircon with detrital cores and four grains with metamorphic dates.

al., 2023). Younger rims (73.7 ± 0.9 Ma) are also observed on zircon from a mica schist, but they have a well-developed negative Eu anomaly that Rubatto et al. (2011) attribute to rim growth at lower-P conditions. The outermost rims of the mica schist zircon show variable flattening of HREE patterns with dates of 77–62 Ma (Rubatto et al., 2011). The observations from zircon suggest that, although the timing of older (78–76 Ma) rim growth may be similar, the trace element signature among samples varies significantly, largely reflecting differences in bulk composition and fluid availability.

Current petrochronologic data from the Eclogitic Micaschist Complex clearly indicate a complicated subduction and exhumation history for the Sesia Zone (Vho et al., 2020). Multiple subduction cycles recorded in single samples have been documented at several localities for peak conditions up to 620 °C and 22 kbar (Rubatto et al., 2011; Regis et al., 2014), which are slightly higher than the P–T estimates obtained here. Domains with differing P–T paths and timing estimates have been proposed as well (Giuntoli et al., 2018). Chen et al.'s (2023) recent report of coesite in the jadeite-bearing orthogneiss, located in the quarry approxi-

mately 2.5 km east of the locality discussed here, raises the additional caveat that portions of the Sesia Zone have experienced UHP conditions at 78–76 Ma. Our conservative estimate for equilibration at 550 ± 50 °C and 18 ± 2 kbar is consistent with the literature (Tropper et al., 1999; Regis et al., 2014), and we have not found evidence for UHP conditions in our samples. However, in light of the high values of measured Si in phengite of ~ 3.38 a.p.f.u. (atoms per formula unit) and j (jd) of ~ 0.90 in clinopyroxene (sample VA1; Table S1), our numbers may be regarded as minimum P–T estimates, without excluding a potential UHP stage preceding the conditions recorded by our samples. In general, the observed variability in metamorphic conditions and ages for the Eclogitic Micaschist Complex is consistent with the structural interpretation that the Sesia Zone consists of numerous tectonic slices separated by shear zones (e.g., Babist et al., 2006; Angiboust et al., 2014; Manzotti et al., 2014a, b; Giuntoli and Engi, 2016). Additional mapping and dating are needed to define the size and extent of individual tectonic slices which are expected in a subduction channel environment.

Data availability. Data beyond what are presented will be made available upon request.

Supplement. The supplement related to this article is available online at: https://doi.org/10.5194/ejm-35-645-2023-supplement.

Author contributions. RC, JAG and WCMC collected samples 15-1 and 15-2; SiS collected VA1. RC, JAG and SiS did the petrology. SiS collected the mineral chemistry data and ran the thermodynamic models. WCMC and MAC analyzed zircon with SHRIMP-RG, while WCMC collected detrital zircon data with the LA-ICP-MS. JAG and WCMC wrote the manuscript with input from all co-authors.

Competing interests. The contact author has declared that none of the authors has any competing interests.

Disclaimer. Publisher's note: Copernicus Publications remains neutral with regard to jurisdictional claims in published maps and institutional affiliations.

Special issue statement. This article is part of the special issue "(Ultra)high-pressure metamorphism, from crystal to orogenic scale". It is a result of the 14th International Eclogite Conference (IEC-14) held in Paris and Lyon, France, 10–13 July 2022.

Acknowledgements. We dedicate this paper to Marco Beltrando, whose brilliant career – though tragically short – is an inspiration to us all. Jane A. Gilotti and William C. McClelland would also like to thank the Department of Earth Sciences at the University of Torino for their gracious hospitality during our sabbatical visit in 2015 when the samples were collected.

Financial support. This research has been supported by the Austrian Science Fund (grant no. P-33002-N) to Simon Schorn.

Review statement. This paper was edited by Gaston Godard and reviewed by Martin Engi and Thomas Gyomlai.

References

Andreoli, M., Compagnoni, R., and Lombardo, B.: Jadeite megablasts from Valchiusella (Sesia-Lanzo zone, Western Alps), Rend. Soc. Ital. Mineral. Petrol., 32, 681–698, 1976.

Angiboust, S., Glodny, J., Oncken, O., and Chopin, C.: In search of transient subduction interfaces in the Dent Blanche–Sesia tectonic system (W. Alps), Lithos, 205, 298–321, 2014.

Arboit, F., Chew, D., Visoná, D., Massironi, M., Sciascia, F., Benedetti, G., and Rodani, S.: The geodynamic evolution of the Italian South Alpine basement from the Ediacaran to the Carboniferous: Was the South Alpine terrane part of the peri-Gondwana arc-forming terranes?, Gondwana Res., 65, 17–30, 2019.

Avigad, D., Weissbrod, T., Gerdes, A., Zlatkin, O., Ireland, T. R., and Morag, N.: The detrital zircon U–Pb–Hf fingerprint of the northern Arabian–Nubian Shield as reflected by a Late Ediacaran arkosic wedge (Zenifim Formation; subsurface Israel), Precambrian Res., 266, 1–11, 2015.

Babist, J., Handy, M. R., Konrad-Schmolke, M., and Hammerschmidt, K.: Precollisional, multistage exhumation of subducted continental crust: The Sesia Zone, western Alps, Tectonics, 25, TC6008, https://doi.org/10.1029/2005TC001927, 2006.

Barth, A. P. and Wooden, J. L.: Timing of magmatism following initial convergence at a passive margin, southwestern U.S. Cordillera, and ages of lower crustal magma sources, J. Geology, 114, 231–245, 2006.

Barth, A. P. and Wooden, J. L.: Coupled elemental and isotopic analyses of polygenetic zircons from granitic rocks by ion microprobe, with implications for melt evolution and the sources of granitic magmas, Chem. Geol., 277, 149–159, 2010.

Beltrando, M., Compagnoni, R., and Lombardo, B.: (Ultra-) High-pressure metamorphism and orogenesis: An Alpine perspective, Gondwana Res., 18, 147–166, 2010a.

Beltrando, M., Rubatto, D., and Manatschal, G.: From passive margins to orogens: The link between ocean-continent transition zones and (ultra)high-pressure metamorphism, Geology, 38, 559–562, 2010b.

Beltrando, M., Manatschal, G., Mohn, G., Dal Piaz, G. V., Brovarone, A. V., and Masini, E.: Recognizing remnants of magma-poor rifted margins in high-pressure orogenic belts: The Alpine case study, Earth-Sci. Rev., 131, 8–115, 2014.

Black, L. P., Kamo, S. L., Allen, C. M., Davis, D. W., Aleinikoff, J. N., Valley, J. W., Mundil, R., Campbell, I. H., Korsch, R. J., Williams, I. S., and Foudoulis, C.: Improved $^{206}Pb/^{238}U$ microprobe geochronology by the monitoring of a trace-element related matrix effect; SHRIMP, ID-TIMS, ELA-ICP-MS and oxygen isotope documentation for a series of zircon standards, Chem. Geol., 205, 115–140, 2004.

Bussy, F., Venturini, G., Hunziker, J. C., and Martinotti, G.: U-Pb ages of magmatic rocks of the Western Austroalpine Dent-Blanche-Sesia Unit, Schweiz. Mineral. Petrogr. Mitt., 78, 163–168, 1998.

Chen, Y.-X., Zhou, K., Qiang, H., Zheng, Y.-F., Schertl, H.-P., and Chen, K.: First finding of continental deep subduction in the Sesia Zone of Western Alps and implications for subduction dynamics, Nat. Sci. Rev., 10, nwad023, https://doi.org/10.1093/nsr/nwad023, 2023.

Coble, M. A., Vazquez, J. A., Barth, A. P., Wooden, J., Burns, D., Kylander-Clark, A., Jackson, S., and Vennari, C. E.: Trace Element Characterisation of MAD-559 Zircon Reference Material for Ion Microprobe Analysis, Geostand. Geoanalyt. Res., 42, 481–497, 2018.

Compagnoni, R. and Maffeo, B.: Jadeite-bearing metagranites l.s. and related rocks in the Monte Mucrone area (Sesia-Lanzo zone, Western Italian Alps), Schweiz. Mineral. Petrogr. Mitt., 53, 355–378, 1973.

Compagnoni, R., Dal Piaz, G. V., Hunziker, J. C., Gosso, G., Lombardo, B., and Williams, P. F.: The Sesia-Lanzo zone, a slice of continental crust with alpine high-pressure–low temperature assemblages in the Western Italian Alps, Rend. Soc. Ital. Mineral. Petrol., 33, 281–334, 1977.

Compagnoni, R., Engi, M., and Regis, D.: Val d'Aosta section of the Sesia Zone: multi-stage HP metamorphism and assembly of a rifted continental margin. 10th Int. Eclogite Conference, Syn-Conference Excursion, 5 September 2013, GFT – Geological Field Trips, 6, 1–44, https://doi.org/10.3301/GFT.2014.02, 2013.

Dachs, E.: PET: petrological elementary tools for Mathematica, Comput. Geosci., 24, 219–235, 1998.

Dal Piaz, G. V.: History of tectonic interpretations of the Alps, J. Geodyn., 32, 99–114, 2001.

Ferry, J. M. and Watson, E. B.: New thermodynamic models and revised calibrations for the Ti-in-zircon and Zr-in-rutile thermometers, Contrib. Mineral. Petrol., 154, 429–437, 2007.

Finger, F., Roberts, M. P., Haunschmid, B., Schermaier, A., and Steyrer, H. P.: Variscan granitoids of central Europe: their typology, potential sources and tectonothermal relations, Mineral. Petrol., 61, 67–96, 1997.

Fiora, L., Fiusello, C., Fornaro, M., and Primavori, P.: Verde Argento, Marmo Macc. Int., 28, 61–82, 1999.

Forshaw, J. B., Waters, D. J., Pattison, D. R. M., Palin, R. M., and Gopon, P.: A comparison of observed and thermodynamically predicted phase equilibria and mineral compositions in mafic granulites, J. Metam. Geol., 37, 153–179, 2019.

Gehrels, G. and Pecha, M.: Detrital zircon U-Pb geochronology and Hf isotope geochemistry of Paleozoic and Triassic passive margin strata of western North America, Geosphere, 10, 49–65, 2014.

Gehrels, G. E., Valencia, V., and Ruiz, J.: Enhanced precision, accuracy, efficiency, and spatial resolution of U-Pb ages by laser ablation-multicollector-inductively coupled plasma-mass spectrometry, Geochem. Geophys. Geosyst. Geochem., 9, Q03017, https://doi.org/10.1029/2007GC001805, 2008.

Gehrels, G., Giesler, D., Olsen, P., Kent, D., Marsh, A., Parker, W., Rasmussen, C., Mundil, R., Irmis, R., Geissman, J., and Lepre, C.: LA-ICPMS U–Pb geochronology of detrital zircon grains from the Coconino, Moenkopi, and Chinle formations in the Petrified Forest National Park (Arizona), Geochronology, 2, 257–282, 2020.

Gibson, T. M., Faehnrich, K., Busch, J. F., McClelland, W. C., Schmitz, M. D., and Strauss, J. V.: A detrital zircon test of large-scale terrane displacement along the Arctic margin of North America, Geology, 49, 545–550, 2021.

Giuntoli, F. and Engi, M.: Internal geometry of the central Sesia Zone (Aosta Valley, Italy): HP tectonic assembly of continental slices, Swiss J. Geosci., 109, 445–471, 2016.

Giuntoli, F., Lanari, P., Burn, M., Kunz, B. E., and Engi, M.: Deeply subducted continental fragments – Part 2: Insight from petrochronology in the central Sesia Zone (western Italian Alps), Solid Earth, 9, 191–222, https://doi.org/10.5194/se-9-191-2018, 2018.

Green, E. C. R., White, R. W., Diener, J. F. A., Powell, R., Holland, T. J. B., and Palin, R. M.: Activity-composition relations for the calculation of partial melting equilibria in metabasic rocks, J. Metam. Geol., 34, 845–869, 2016.

Handy, M. R., Schmid, S. M., Bousquet, R., Kissling, E., and Bernoulli, D.: Reconciling plate-tectonic reconstructions of Alpine Tethys with the geological–geophysical record of spreading and subduction in the Alps, Earth Sci. Rev., 102, 121–158, 2010.

Hayden, L. A. and Watson, E. B.: Rutile saturation in hydrous siliceous melts and its bearing on T-thermometry of quartz and zircon, Earth Planet. Sc. Lett., 258, 561–568, 2007.

Holland, T. J. B. and Powell, R.: Activity–composition relations for phases in petrological calculations: an asymmetric multicomponent formulation, Contrib. Mineral. Petrol., 145, 492–501, 2003.

Holland, T. J. B. and Powell, R.: An improved and extended internally consistent thermodynamic dataset for phases of petrological interest, involving a new equation of state for solids, J. Metam. Geol., 29, 333–383, 2011.

Hunziker, J. C.: Rb-Sr and K-Ar age determination and the Alpine tectonic history of the western Alps, Mem. Instituti Geologia e Mineralogia Univ. Padova, 31, 1–45, 1974.

Kunz, B. E., Manzotti, P., von Niederhäusern, B., Engi, M., Darling, J. R., Giuntoli, F., and Lanari, P.: Permian high-temperature metamorphism in the Western Alps (NW Italy), Int. J. Earth Sci., 107, 203–229, 2018.

Liermann, H.-P., Isachsen, C., Altenberger, U., and Oberhänsli, R.: Behavior of zircon during high-pressure, low-temperature metamorphism: Case study from the Internal Unit of the Sesia Zone (Western Italian Alps), Eur. J. Mineral., 14, 61–71, 2002.

Linnemann, U., Pereira, F., Jeffries, T. E., Drost, K., and Gerdes, A.: The Cadomian Orogeny and the opening of the Rheic Ocean: the diachrony of geotectonic processes constrained by LA-ICP-MS U-Pb zircon dating (Ossa-Morena and Saxo-Thuringian Zones, Iberian and Bohemian Massifs), Tectonophysics, 461, 21–43, 2008.

Ludwig, K. R.: Isoplot 3.6, Berkeley Geochronology Center Special Publication 4, 77 pp., 2008.

Ludwig, K. R.: Squid 2: A User's Manual, Berkeley Geochronology Center Special Publication 5, 110 pp., 2009.

Malusà, M. G., Guillot, S., Zhao, L., Paul, A., Solarino, S., Dumont, T., Schwartz, S., Aubert, C., Baccheschi, P., Eva, E., Lu, Y., Lyu, C., Pondrelli, S., Salimbeni, S., Sun, S., and Yuan, W.: The deep structure of the Alps based on the CIFALPS seismic experiment: a synthesis, Geochem. Geophys. Geosyst., 22, e2020GC009466, https://doi.org/10.1029/2020GC009466, 2021.

Manzotti, P., Ballèvre, M., Zucali, M., Robyr, M., and Engi, M.: The tectonometamorphic evolution of the Sesia–Dent Blanche nappes (internal Western Alps): review and synthesis, Swiss J. Geosci., 107, 309–336, 2014a.

Manzotti, P., Zucali, M., Ballèvre, M., Robyr, M., and Engi, M.: Geometry and kinematics of the Roisan-Cignana shear zone, and the evolution of the Dent Blanche Tectonic System (Western Alps), Swiss J. Geosci., 107, 23–47, 2014b.

Massonne, H.-J. and Sobiech, M.: Paragonite: why is it so rare in medium-temperature high-pressure rocks?, Int. Geol. Rev., 49, 301–312, 2007.

Mattinson, J. M.: Analysis of the relative decay constants of ^{235}U and ^{238}U by multi-step CA-TIMS measurements of closed-system natural zircon samples, Chem. Geol., 275, 186–198, 2010.

McClelland, W. C. and Lapen, T. J.: Linking time to the pressure-temperature path for ultrahigh-pressure rocks, Elements, 9, 273–279, 2013.

Meinhold G., Bassis A., Hinderer M., Lewin A., and Berndt J.: Detrital zircon provenance of north Gondwana Palaeozoic sandstones from Saudi Arabia, Geol. Mag., 158, 442–458, 2021.

Nance, D. R., Murphy, J. B., Strachan, R. A., Keppie, J. D., Gutiérrez-Alonso, G., Fernández-Suárez, J., Quesada, C., Linnemann, U., D'Lemos, R., and Pisarevsky, S. A.: Neoproterozoic–early Palaeozoic tectonostratigraphy and palaeogeography of the peri-Gondwanan terranes: Amazonian v. West African connections, in: The Boundaries of the West African Craton, edited by: Ennih, N. and Liégeois, J.-P., Geol. Soc., London, Special Publications, 297, 345–383, 2008.

Paces, J. B. and Miller Jr., J. D.: Precise U-Pb ages of Duluth complex and related mafic intrusions, northeastern Minnesota: Geochronological insights to physical, petrogenetic, paleomagnetic, and tectonomagmatic processes associated with the 1.1 Ga midcontinent rift system, J. Geophys. Res., 98, 13997–14013, 1993.

Paul, A., Malusà, M. G., Solarino, S., Salimbeni, S., Eva, E., Nouibat, A., Pondrelli, S., Aubert, C., Dumont, T., Guillot, S., Schwartz, S., and Zhao, L.: Along-strike variations in the fossil subduction zone of the Western Alps revealed by the CIFALPS seismic experiments and their implications for exhumation of (ultra-) high-pressure rocks, Earth Planet. Sc. Lett., 598, 117843, https://doi.org/10.1016/j.epsl.2022.117843, 2022.

Polino, R., Dal Piaz, G. V., and Gosso, G.: Tectonic erosion at the Adria margin and accretionary processes for the Cretaceous orogeny of the Alps, Mém. Société Géol. France, 156, 345–367, 1990.

Powell, R. and Holland, T. J. B.: An internally consistent thermodynamic dataset with uncertainties and correlations: 3. Application, methods, worked examples and a computer program, J. Metam. Geol., 6, 173–204, 1988.

Regis, D., Rubatto, D., Darling, J., Cenki-Tok, B., Zucali, M., and Engi, M.: Multiple metamorphic stages within an eclogite-facies terrane (Sesia Zone, western Alps) revealed by Th–U–Pb petrochronology, J. Petrol., 55, 1429–1456, 2014.

Rubatto, D.: Dating of Pre-Alpine Magmatism, Jurassic Ophiolites and Alpine Subductions in the Western Alps, PhD thesis (unpublished), ETH, Swiss Federal Institute of Technology, 1998.

Rubatto, D., Regis, D., Hermann, J., Boston, K., Engi, M., Beltrando, M., and McAlpine, S. R. B.: Yo-yo subduction recorded by accessory minerals in the Italian Western Alps, Nat. Geosci., 4, 338–342, 2011.

Schaltegger, U. and Gebauer, D.: Pre-Alpine geochronology of the Central, Western and Southern Alps, Schweiz. Mineral. Petrogr. Mitt., 79, 79–87, 1999.

Siegesmund, S., Oriolo, S., Broge, A., Hueck, M., Lammerer, B., Basei, M. A. S., and Schulz, B.: Cadomian to Cenerian accretionary orogenic processes in the Alpine basement: the detrital zircon archive, Int. J. Earth Sci., 112, 1157–1174, https://doi.org/10.1007/s00531-023-02305-6, 2023.

Sirevaag, H., Jacobs, J., Ksienzyka, A. K., Rocchi, S., Paoli, G., Jørgensen, H., and Košler, J.: From Gondwana to Europe: The journey of Elba Island (Italy) as recorded by U–Pb detrital zircon ages of Paleozoic metasedimentary rocks, Gondwana Res., 38, 273–288, 2016.

Stacey, J. S. and Kramers, J. D.: Approximation of terrestrial lead isotope evolution by a two stage model, Earth Planet. Sc. Lett., 26, 207–221, 1975.

Tropper P., Essene E. J., Sharp Z. D., and Hunziker, J. C.: Application of K-feldspar – jadeite-quartz barometry to eclogite facies metagranites and metapelites in the Sesia Lanzo Zone (Western Alps, Italy), J. Metam. Geol., 17, 195–209, 1999.

Venturini, G., Martinotti, G., Armando, G., Barbero, M., and Hunziker, J. C.: The Central Sesia Lanzo zone (Western Italian Alps): new field observations and lithostratigraphic subdivisions, Schweiz. Mineral. Petrogr. Mitt., 74, 115–125, 1994.

Vho, A., Rubatto, D., Lanari, P., and Regis, D.: The evolution of the Sesia Zone (Western Alps) from Carboniferous to Cretaceous: insights from zircon and allanite geochronology, Swiss J. Geosci. 113, https://doi.org/10.1186/s00015-020-00372-4, 2020.

von Raumer, J. F., Bussy, F., Schaltegger, U., Schulz, B., and Stampfli, G. M.: Pre-Mesozoic Alpine basements – their place in the European Paleozoic framework, Geol. Soc. Am. Bull., 125, 89–108, 2013.

von Raumer, J. F., Stampfli, G. M., Arenas, R., and Martínez, S. S.: Ediacaran to Cambrian oceanic rocks of the Gondwana margin and their tectonic interpretation, Int. J. Earth Sci., 104, 1107–1121, 2015.

Watson, E. B., Wark, D. A., and Thomas, J. B.: Crystallization thermometers for zircon and rutile, Contrib. Mineral. Petrol., 151, 413–433, 2006.

White, R. W., Powell, R., Holland, T. J. B., Johnson, T. E., and Green, E. C. R.: New mineral activity-composition relations for thermodynamic calculations in metapelitic systems, J. Metam. Geol., 32, 261–286, 2014a.

White, R. W., Powell, R., and Johnson, T. E.: The effect of Mn on mineral stability in metapelites revisited: new a–x relations for manganese-bearing minerals, J. Metam. Geol., 32, 809–828, 2014b.

Whitney, D. L. and Evans, B. W.: Abbreviations for names of rock-forming minerals, Am. Mineralogist, 95, 185–187, 2010.

Williams, I. S.: U–Pb by ion microprobe, in: Applications of micro-analytical techniques to understanding mineralizing processes, edited by: McKibben, M. A., Shanks, W. C., and Ridley, W. I., Soc. Econ. Geol. Rev. Econ. Geol., 7, 1–35, 1998.

Žák, J., Svojtka, M., Gerdjikov, I., Kounov, A., and Vangelov, D. A.: The Balkan terranes: a missing link between the eastern and western segments of the Avalonian–Cadomian orogenic belt?, Int. Geol. Rev., 64, 2389–2415, 2022.

Zucali, M., Spalla, M. I., and Gosso, G.: Strain partitioning and fabric evolution as a correlation tool: the example of the Eclogitic Micaschists Complex in the Sesia-Lanzo Zone (Monte Mucrone-Monte Mars, Western Alps, Italy), Schweiz. Mineral. Petrogr. Mitt., 82, 429–454, 2002.

Zurbriggen, R.: Ordovician orogeny in the Alps: a reappraisal, Int. J. Earth Sci., 104, 335–350, 2015.